Chirality

DOI: 10.1002/anie.201303023

Three-Dimensional Near-Surface Imaging of Chirality Domains with Circularly Polarized X-rays**

Hiroyuki Ohsumi, Akihisa Tokuda, Soshi Takeshita, Masaki Takata, Motohiro Suzuki, Naomi Kawamura, Yusuke Kousaka, Jun Akimitsu, and Taka-hisa Arima*

The homochirality of biological molecules, exclusively left-handed amino acids and right-handed sugars, is essential for life processes such as the protein function of specific molecular recognition and DNA replication. Therefore, the absolute configuration of a chiral molecule is crucial for understanding the difference in biological activity between enantiomers. X-ray crystallography is the most common method of absolute structure determination, based on the violation of Friedel's law because of the anomalous dispersion effect.[1] Chirality-related activities are also expected in nonbiological system if enantiomeric excess exists. An enantiopure crystal is the ideal form of functional materials having chirality-related activities like a second-harmonic generation crystal. Chiral crystallization itself is a fascinating phenomenon allowing straightforward and efficient segregation of enantiomers, which is essential in pharmaceutical industry so as to extract beneficial biological activities. However, the majority of racemates, mixtures of enantiomers, crystallize in a racemic twin but not in a conglomerate of enantiopure crystals. The exact reason for this is not fully understood yet, and therefore the formation of conglomerates cannot be predicted a priori.[2]

A microscopical examination of domain morphology is useful for establishing the regulation scheme of enantiopure crystal growth. In particular, a depth profile is crucial for understanding the enantioselectivity on surfaces. By means of chiroptical techniques (e.g. measurement of natural optical activity and circular dichroism), however, it is difficult to obtain the depth profile near the crystal growth front since all the effects are averaged along the light path. X-rays provide a definitive method to determine the absolute configuration as mentioned above. As for enantiopurity, respective fractions of enantiomers are evaluated by examining the Flack parameter.[3] However, the size of a sample crystal is strongly restricted so as to meet the $\mu R < 1$ criterion, where μ and R are the linear X-ray absorption coefficient and the crystal radius, respectively. One cannot determine the chirality-domain distribution on a large crystal surface through an X-ray crystal structure analysis.

An X-ray screw-axis ATS reflection (here ATS denotes the anisotropy of the tensor of susceptibility)[4] provides a plain procedure for enantiomorph identification. Near X-ray absorption edges the ATS is enhanced and some forbidden reflections gain a measurable intensity. The handedness of the screw is simply examined by comparing a forbidden reflection intensity between left- and right-handed circularly polarized incident X-rays.[5,6] A dark-field imaging of chirality-domain distribution in a racemic solid solution can be realized by using circularly polarized and finely focused X-rays. In addition, we focus attention on the fact that the penetration depth of X-ray drastically varies with photon energy close to an absorption edge, which enables us to obtain a depth profile of the chirality near the crystal growth front.

To demonstrate this method practically, we imaged a near-surface chirality-domain distribution in a $CsCuCl_3$ crystal. $CsCuCl_3$ is a hexagonal perovskite system belonging to an achiral space group $P6_3/mmc$ at high temperatures. Below $T_C = 423$ K, the Jahn–Teller effect on Cu^{2+} ions induces cooperative atomic displacements and results in lowering of lattice symmetry to $P6_122$ or $P6_522$ which are enantiomorphous each other (Figure 1a).[7] Near the Cu K edge, $00l$ ($l = 6n \pm 2$) reflections being forbidden because of 6_1 and 6_5 screw axes are excited and their intensities depend on the degree of circular polarization P_C of incident X-ray, where $P_C = +1$ and $P_C = -1$ correspond to the right- and left-handed circular polarizations, respectively. Intensity of the $00l$ ($l = 6n \pm 2$) reflections from a $P6_122$ crystal is given[6] by $A\cdot(1+\sin^2\theta)(1\mp P_C\sin\theta)^2$ where θ is the Bragg angle and A is independent of P_C (see the Supporting Information). The double sign is reversed to $\pm$ for a $P6_522$ crystal.

In the experimental implementation of this concept, linearly polarized X-rays from a planar undulator insertion

[*] Dr. H. Ohsumi, Dr. S. Takeshita, Prof. M. Takata, Prof. T. Arima
RIKEN SPring-8 Center, Sayo, Hyogo 679-5148 (Japan)
E-mail: ohsumi@spring8.or.jp
A. Tokuda
Department of Physics, Kwansei Gakuin University
Sanda, Hyogo 669-1337 (Japan)
Prof. T. Arima
Department of Advanced Materials Science, University of Tokyo
Kashiwa, Chiba 277-8561 (Japan)
Prof. M. Takata, Dr. M. Suzuki, Dr. N. Kawamura
Japan Synchrotron Radiation Research Institute/SPring-8
Sayo, Hyogo 679-5198 (Japan)
Dr. Y. Kousaka, Prof. J. Akimitsu
Department of Physics and Mathematics
Aoyama-Gakuin University
Sagamihara, Kanagawa 252-5258 (Japan)

[**] This work was supported by the MEXT of Japan through a grant-in-aid for exploratory research (grant number 19654046). This work was performed at BL39XU in SPring-8 with the approval of the Japan Synchrotron Radiation Research Institute (JASRI) (proposal numbers 2009A1607, 2009B1586). We acknowledge Y. Nakao, T. Yokobori and H. Matsui for their help in the synchrotron radiation experiment. We also thank S. Tardif for comments regarding a draft of this manuscript.

Supporting information for this article is available on the WWW under http://dx.doi.org/10.1002/anie.201303023.

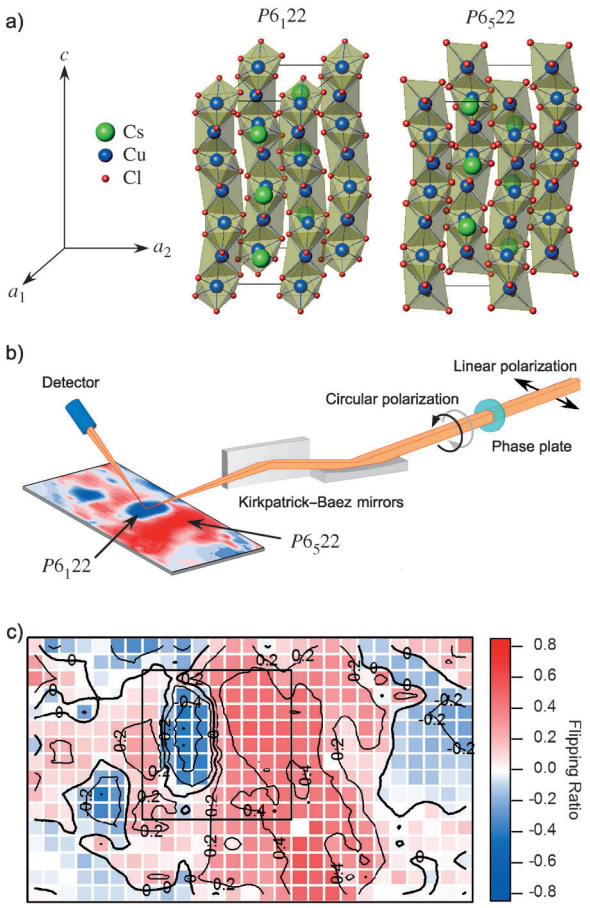

Figure 1. a) Enantiomorphic crystal structures of $CsCuCl_3$ below T_C. Large, medium, and small spheres represent Cs, Cu, and Cl, respectively. b) A X-ray phase plate converts linear polarization to circular one. The Kirkpatrick–Baez mirrors focus the circularly polarized X-ray on the sample. The sample crystal is scanned through the beam. c) The 00*l* ($l=14$) screw axis forbidden reflection dark field image (270×160 μm^2 with 10 μm steps). The scale is denoted by the color bar. The high resolution image (90×90 μm^2 with 5 μm steps) of the framed square area is given in Figure S1.

device were monochromatized to a photon energy near the Cu *K*-edge and were converted to circular polarization by using a diamond phase retarder.[8] Kirkpatrick–Baez mirrors[9,10] focused the circularly polarized X-rays down to 2.7×2.7 μm^2 at the sample position (Figure 1b). The irradiation area on a sample surface was scanned by shifting the translational position of the whole diffractometer. To obtain chirality-domain images, the diffractometer was scanned perpendicular to the beam. At each position, the intensity of a forbidden reflection 00*l* ($l=14$) was measured with circularly polarized beams; $I(P_C{=}\pm1)$ denotes the intensity for right- and left-handed circular polarization, respectively. The flipping ratio, defined in Equation (1),

$$R=\frac{I(P_C=+1)-I(P_C=-1)}{I(P_C=+1)+I(P_C=-1)} \quad (1)$$

is a good measure of the enantiopurity of the position, because the *R* value is directly related to volume fractions of respective domains, $\Phi(P6_122)$ and $\Phi(P6_522)$. For the 00*l* ($l=14$) reflection, the flipping ratio is written as given in Equation (2).

$$R=-\frac{2\sin\theta}{1+\sin^2\theta}[\Phi(P6_122)-\Phi(P6_522)] \quad (2)$$

Flipping ratio variation on a cleaved (001) surface of $CsCuCl_3$ was measured by scanning the sample crystal in 10 μm steps over 270×160 μm^2 with X-rays of 8.986 keV (Figure 1c). The blue-tinged region corresponds to a negative *R* domain having a 6_1 screw axis. The domain having the opposite handedness of the screw axis is shown as red-tinged region. The observed chirality-domain distribution was of racemic solid solution and the typical domain size was several tens of microns. At each step, rocking curves of the 00*l* ($l=14$) forbidden reflection were measured for right- and left-handed circularly polarized incident X-rays (see Figure S1 in the Supporting Information), which required 90 seconds. The flipping ratio *R* was evaluated from integrated intensities for both polarizations. The enantiopure $P6_122$ ($P6_522$) crystal gives $R=-0.83$ ($+0.83$) for the 00*l* ($l=14$) forbidden reflection at $\theta=32.1°$ where the polarization is completely circular. These procedures provide a quantitative flipping ratio but require a long time; the data acquisition time for Figure 1c was 648 min, for instance.

The observed *R* values are rather small compared to the expectation values for enantiopure crystals. Since each chirality domain gives either the positive or negative expectation *R* value, an intermediate *R* value means the existence of multiple domains within the beam spot. The lateral domain size, however, seems much larger than the beam spot size. Therefore, alternation of chirality domains is expected along the longitudinal direction and it is necessary to analyze a depth profile for further understanding of chirality-domain morphology.

X-rays have the ability to penetrate into a matter. Here we define the penetration depth *d* as the skin depth where 95.4% of the reflection intensity comes from, then the penetration depth is expressed as [Eq. (3)],

$$d=\frac{\sin\theta}{2\mu(E)}\ln\frac{1}{1-0.954} \quad (3)$$

where $\mu(E)$ is the linear X-ray absorption coefficient. Figure 2a shows the experimentally determined penetration depth of the 00*l* ($l=14$) reflection and $\mu(E)$ measured in fluorescence-yield mode. A steep change in the penetration depth around the Cu *K* edge enables us to analyze the depth profile of enantiopurity. Flipping ratio maps of the same area (top surfaces of Figure 2b–e) were measured in 2 μm steps over 40×10 μm^2 with X-rays having various photon energies: b) 8.992 keV, c) 8.987 keV, d) 8.985 keV, and e) 8.984 keV. Differences among the flipping ratio maps arise from variation in the penetration depth, not from change in the shape of the *R* spectrum. Since *R* keeps a constant value over the energy range of interest (see Figure S2), the sign reversal of *R* is a direct consequence of interchange of the dominant enantiomer within the penetration depth. At each step, only the peak intensities of the 00*l* ($l=14$) reflection were

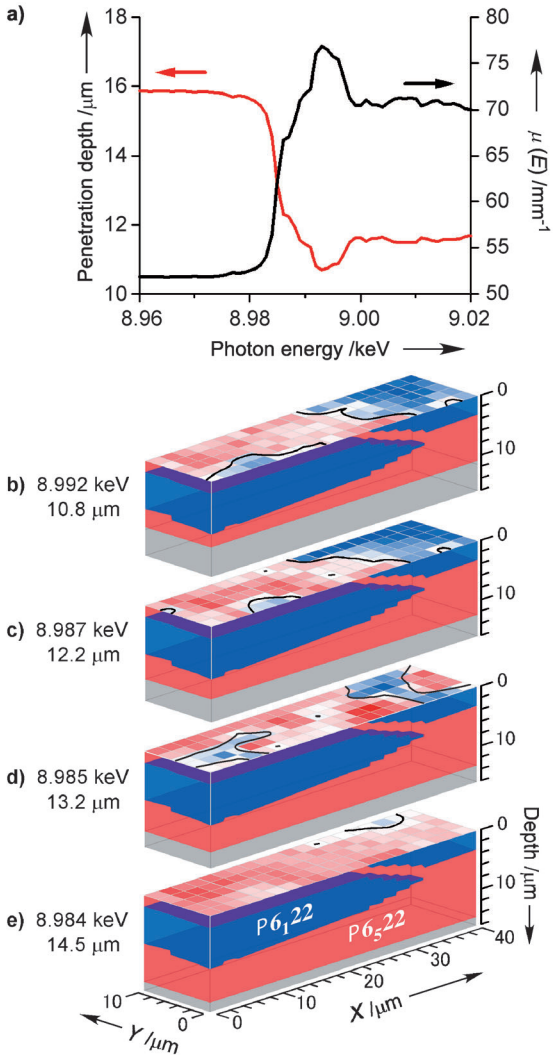

Figure 2. The reconstructed three-dimensional near-surface image of the chirality-domain distribution in the $CsCuCl_3$ crystal. a) The penetration depth of the 00*l* ($l=14$) reflection and the linear X-ray absorption coefficient of $CsCuCl_3$. The top surfaces are flipping ratio maps ($40\times10\ \mu m^2$ with 2 μm steps) obtained at different photon energies: b) 8.992 keV, c) 8.987 keV, d) 8.985 keV, and e) 8.984 keV. The penetration depths of b) 10.8 μm, c) 12.2 μm, d) 13.2 μm, and e) 14.5 μm are schematically shown by colorization for the reconstructed tomographic image of the chirality-domain distribution.

measured for right- and left-handed circularly polarized incident X-rays, which reduced the data acquisition time to 400 seconds for each image. The lack of peak profiles makes the flipping ratio underestimated in magnitude because of residual backgrounds. Despite this drawback, the physical situations specified by zero and the sign of R remain unchanged. For zero crossing pixels in Figure 2b–e, possible depth profiles are easily deduced (see the Supporting Information) and are strongly restricted from the interrelation among themselves. Choosing the simplest layered structure that can account for all the data, one can build up the three-dimensional data from the depth profiles.

The reconstructed three-dimensional chirality-domain distribution under the $CsCuCl_3$ (001) surface (tomographic image of Figure 2b–e) exposes morphological features: a domain boundary parallel to the hexagonal *c* plane is favored; the typical domain size is several tens of microns laterally and only a few microns thick. A shallow domain shape perpendicular to the *c* axis is in contrast to an outer shape of an as-grown crystal with faces of the hexagonal prism {100} and hexagonal bipyramids {*h*0*l*}. The possibility of a facet would be attributed to nonpolar surface termination: stacking of neutral $CuCl_2$ and CsCl layers results in the nonpolar {100} facet and formation of step-terrace structures on the {100} surface yields the {*h*0*l*} facet. One can find stacking of neutral $Cs_{2n}Cu_{2n-1}Cl_{6n-2}$ and $CuCl_2$ building blocks in a nonpolar {*n*03} surface, whereas the {110} layer of $CsCuCl^{2+}/Cl_2^{2-}$ and the (001) layer of $Cu^{2+}/CsCl_3^{2-}$ give rise to polar surface termination.

The observed shallow chirality-domain shape suggests that in-plane dislocations are much more difficult to be induced than out-of-plane dislocations. The difference between enantiomers appears to be handedness of helices formed by lateral displacements of (001) atomic layers around the screw axis (Figure 1a). $CuCl_6$ octahedra, which elongate approximately 20% along one body diagonal, pile up along the *c* axis by sharing common faces and uniformly align within the *c* plane direction. Therefore, relatively high in-plane cooperativity of Jahn–Teller distortion of $CuCl_6$ octahedra is considered to be the predominant factor determining the shape of a chirality domain in this material. As demonstrated above, observation of chirality-domain morphology is quite essential to understand conflict between enantiomers and can provide clues for a regulation scheme of enantiopure crystal growth.

Recently, chiral crystallization of magnetic materials attracts much attention, since simultaneous violation of time and space inversion symmetry evokes unusual electromagnetic phenomena such as multiferroics[11] and skyrmion crystal.[12] Nonbiological chirality-related activities are of growing interest also in the field of catalysts and for optical materials. For facilitating a further discovery of intriguing materials and phenomena, an enantiopure chiral crystal is advantageous over racemic twins, because chirality-related activities are compensated between enantiomers. However, there is no universal guiding principle for growing an enantiopure chiral crystal consisting of achiral ionic components, whereas chirality-selective crystallization of molecular-based materials is feasible by using the stereochemical nature of molecules. The newly developed technique enables us to investigate chirality-domain morphology and leads to a deeper understanding of enantiopure crystal growth, which itself is an interesting issue relating to chiral autocatalytic growth under non-equilibrium conditions as seen in $NaClO_3$.[13,14]

In summary, we have successfully imaged chirality domains in a $CsCuCl_3$ crystal by means of circularly polarized resonant X-ray microdiffraction. Near absorption edges X-ray susceptibility becomes anisotropic and allows us to distinguish enantiomers by using circular polarization. In addition to the surface observation as a scanning probe microscope using a focused X-ray beam, nondestructive depth profile analysis is also achieved by controlling an X-

ray penetration depth. The three-dimensional near-surface imaging technique facilitates investigation of the chirality-domain morphology and the underlying twining mechanisms, which will advance the crystal engineering of enantiopure crystalline substances, potential materials having various beneficial functionalities.

Received: April 11, 2013
Published online: July 1, 2013

Keywords: analytical methods · chirality · scanning probe microscopy · X-ray diffraction

[1] J. M. Bijvoet, A. F. Peerdeman, A. J. van Bommel, *Nature* **1951**, *168*, 271 – 272.
[2] L. Pérez-García, D. B. Amabilino, *Chem. Soc. Rev.* **2002**, *31*, 342 – 356.
[3] H. D. Flack, *Acta Crystallogr. Sect. A* **1983**, *39*, 876 – 881.
[4] V. E. Dmitrienko, *Acta Crystallogr. Sect. A* **1983**, *39*, 29 – 35.
[5] Y. Tanaka, T. Takeuchi, S. W. Lovesey, K. S. Knight, A. Chainani, Y. Takata, M. Oura, Y. Senba, H. Ohashi, S. Shin, *Phys. Rev. Lett.* **2008**, *100*, 145502.
[6] Y. Kousaka, H. Ohsumi, T. Komesu, T. Arima, M. Takata, S. Sakai, M. Akita, K. Inoue, T. Yokobori, Y. Nakao, E. Kaya, J. Akimitsu, *J. Phys. Soc. Jpn.* **2009**, *78*, 123601.
[7] A. W. Schlueter, R. A. Jacobson, R. E. Rundle, *Inorg. Chem.* **1966**, *5*, 277 – 280.
[8] K. Hirano, K. Izumi, T. Ishikawa, S. Annaka, S. Kikuta, *Jpn. J. Appl. Phys.* **1991**, *30*, L407 – L410.
[9] M. Takagaki, M. Suzuki, N. Kawamura, H. Mimura, T. Ishikawa, *Proc. 8th Int. Conf. X-ray Microscopy, IPAP Conf. Series* **2006**, *7*, 267 – 269.
[10] H. Yumoto, K. Hirata, A. Nisawa, G. Ueno, M. Sato, J.-Y. Son, T. Koganezawa, M. Machida, T. Muro, I. Hirosawa, M. Suzuki, N. Kawamura, M. Mizumaki, H. Ohashi, M. Yamamoto, Y. Watanabe, S. Goto, *Proc. SPIE-Int. Soc. Opt. Eng.* **2009**, *7448*, 74480Z-1.
[11] W. Eerenstein, N. D. Mathur, J. F. Scott, *Nature* **2006**, *442*, 759 – 765.
[12] X. Z. Yu, Y. Onose, N. Kanazawa, J. H. Park, J. H. Han, Y. Matsui, N. Nagaosa, Y. Tokura, *Nature* **2010**, *465*, 901 – 904.
[13] D. K. Kondepudi, R. J. Kaufman, N. Singh, *Science* **1990**, *250*, 975 – 976.
[14] C. Viedma, *Phys. Rev. Lett.* **2005**, *94*, 065504.

